ORIGINAL SCIENTIFIC PAPER

CROATICA CHEMICA ACTA

Croat. Chem. Acta **2026**, *99*(4)
Published online: November 20, 2026
DOI: 10.5562/cca4402

HKD 1926

Comparative *in vivo* Safety Assessment of Surface-Engineered Gold Nanocarriers for Oral L-DOPA Delivery

Filip Vrban,[1,2] Vedran Dovečer,[3,4] Petra Dolenec,[4] Anamaria Gojanović Rajić,[5] Maja Beus,[5] Lucija Božičević,[5] Nikolina Kalčec,[5] Nikolina Peranić,[5] Antonija Sulimanec,[5] Jasna Jurasović,[5] Ruža Frkanec,[6] Vedran Micek,[5] Krešimir Rotim,[7,8] Ivana Vinković Vrček[4,5,*]

[1] Clinical Hospital Center Sestre Milosrdnice, Zagreb, Croatia
[2] J. J. Strossmayer University of Osijek, Faculty of Medicine, Osijek, Croatia
[3] General Hospital Varaždin, Varaždin, Croatia
[4] University of Rijeka, Faculty of Medicine, Rijeka, Croatia
[5] Institute for Medical Research and Occupational Health, Zagreb, Croatia
[6] University of Zagreb, Centre for Research and Knowledge Transfer in Biotechnology, Zagreb, Croatia
[7] Neurospine Special Hospital, Zagreb, Croatia
[8] University of Applied Health Sciences, Zagreb, Croatia
* Corresponding author's e-mail address: ivinkovic@imi.hr

RECEIVED: August 04, 2026 * REVISED: September 15, 2026 * ACCEPTED: September 30, 2026

THIS PAPER IS DEDICATED TO THE MEMORY OF OLGA KRONJA (1953 – 2025)

Abstract: Gold nanoparticles (AuNPs) are among the most extensively investigated nanomaterials for targeted drug delivery owing to their unique physicochemical properties, versatile surface functionalisation, and potential to transport therapeutics across biological barriers. However, comprehensive *in vivo* safety data following repeated oral exposure remain limited, particularly for surface-stabilised AuNP formulations intended for oral drug delivery. In this study, we performed a comparative *in vivo* safety assessment of two AuNP formulations synthesized in the presence of peptidoglycan monomer (PGM) or adamantane (Ad), administered alone or following pre-incubation with L-DOPA, in healthy male and female Wistar Han rats.

Animals received test substances daily by oral gavage for 28 days. Gold accumulation in major organs was quantified by inductively coupled plasma mass spectrometry (ICP-MS), and systemic safety was assessed by serum biochemical analyses together with measurements of reactive oxygen species (ROS) and reduced glutathione (GSH) in serum, liver, kidneys, and brain.

Repeated oral administration resulted in measurable, organ-specific gold accumulation, predominantly in the kidney and liver, without significant main effect of sex or treatment ×sex interaction on tissue distribution; gold was not detected in brain tissue. Biochemical alterations were more pronounced following Ad-AuNP administration, whereas PGM-AuNP exposure produced only limited changes in serum biochemical parameters. Mild changes in selected liver and kidney biomarkers were observed in some treatment groups but were not consistently accompanied by oxidative stress or widespread systemic toxicity, and tissue ROS and GSH levels indicated only modest redox perturbations.

These findings indicate that repeated oral exposure to PGM-AuNPs can result in organ-specific gold accumulation without marked systemic toxicity in healthy rats. Despite comparable primary size, morphology, hydrodynamic diameter, and ζ-potential, PGM-AuNPs and Ad-AuNPs elicited distinct biological responses, indicating that tissue gold burden and conventional physicochemical descriptors alone do not predict their *in vivo* biological behaviour. The favourable safety profile of PGM-AuNPs supports their continued preclinical development as oral L-DOPA nanocarriers, while pharmacokinetics, brain delivery efficiency, and therapeutic efficacy remain to be established in subsequent studies.

Keywords: nanosafety, gold nanoparticles, adamantane, peptidoglycan monomer, L-DOPA, Wistar rat.

INTRODUCTION

NEURODEGENERATIVE disorders are among the fastest-growing causes of disability and mortality worldwide, largely driven by population ageing and increasing life expectancy.[1] Despite remarkable advances in understanding the molecular mechanisms underlying these diseases, the translation of this knowledge into effective

This work is licensed under a Creative Commons Attribution 4.0 International License.

therapies has remained disappointingly slow.[2] Parkinson's disease (PD), the second most prevalent neurodegenerative disorder after Alzheimer's disease, exemplifies this challenge.[3] Although several pharmacological agents are available to alleviate symptoms, their long-term therapeutic efficacy is limited by poor delivery to the central nervous system (CNS) and dose-limiting systemic adverse effects.[3,4] The principal obstacle is the blood-brain barrier (BBB), a highly selective physiological interface that protects the brain from circulating xenobiotics but simultaneously prevents the entry of approximately 98 % of small-molecule drugs and nearly all biological therapeutics.[2,5] Achieving sufficient brain drug concentrations while minimising off-target exposure therefore remains one of the greatest challenges in the development of safe and effective therapies for PD and other neurodegenerative disorders.

Nanotechnology has emerged as a promising strategy to overcome the limitations of conventional CNS drug delivery by enabling the rational design of nanocarriers with tailored physicochemical properties.[6] Unlike free drug molecules, nanocarriers can protect therapeutics from premature degradation, improve their pharmacokinetic profile, prolong systemic circulation, and enable controlled or stimuli-responsive drug release. Surface engineering further allows functionalisation with targeting ligands or biomolecules that enhance transport across the BBB and promote selective accumulation at diseased tissues, thereby increasing therapeutic efficacy while reducing off-target exposure and systemic toxicity.[4,5] These multifunctional capabilities have positioned nanocarrier-based delivery systems among the most promising approaches for improving the treatment of neurodegenerative disorders.[7]

Among the various strategies for engineering gold nanoparticle (AuNP) surfaces, ligand selection is particularly important because surface chemistry governs colloidal stability, interactions with biological molecules, cellular uptake, biodistribution, and ultimately biological responses. In the present study, two structurally distinct ligands were selected to stabilise AuNPs. Adamantane is a rigid, highly hydrophobic cage-like molecule that has been extensively explored in medicinal chemistry owing to its favourable membrane interactions and its presence in clinically used antiviral and antiparkinsonian drugs, such as amantadine. In contrast, peptidoglycan monomer (PGM) is a naturally occurring peptidoglycan monomer that has been investigated as a biologically compatible ligand because of its hydrophilicity and multiple functional groups enabling stable surface stabilisation. These markedly different physicochemical characteristics provided an opportunity to investigate how nanoparticle surface chemistry influences drug loading, biological interactions, biodistribution, and systemic safety following repeated oral administration.

Building on these complementary surface chemistries, we previously adopted a rational design approach to develop and optimize AuNP-based nanocarriers for PD therapy by systematically comparing several stabilization strategies, including polyethylene glycol (PEG), 1-adamantylamine, 1-adamantylglycine, and peptidoglycan monomer (PGM). We and found that surface chemistry profoundly influenced drug binding, colloidal stability, and interactions with serum proteins, with PGM-AuNPs showing the highest affinity and loading efficiency for L-DOPA and dopamine.[8] These findings highlighted PGM as a particularly promising coating for brain-targeted drug delivery while simultaneously demonstrating that nanoparticle surface stabilization is a key determinant of nanocarrier performance, warranting comparative *in vivo* evaluation of different surface-engineered formulations.[8] Furthermore, PGM coating preserved drug binding in the presence of serum albumin, indicating enhanced stability under biologically relevant conditions and suggesting favourable performance *in vivo*.[9] These findings identified PGM-AuNPs as the most promising candidate for brain-targeted drug delivery and provided the rationale for advancing this nanocarrier platform to preclinical *in vivo* evaluation.[8] However, the same physicochemical characteristics that govern nanoparticle transport, cellular uptake, and biological interactions also determine their biodistribution, persistence, and potential toxicological effects. Although surface chemistry is recognised as one of the principal determinants of nanoparticle behaviour, few studies have systematically compared the *in vivo* biological responses induced by different surface-engineered AuNP formulations and their corresponding drug-loaded counterparts under identical experimental conditions.[10] Consequently, comprehensive *in vivo* assessment remains indispensable before considering further efficacy studies in disease models.

The present study represents the next stage in the preclinical development of rationally designed AuNP-based nanocarriers for Parkinson's disease therapy. The continued interest in AuNP-based L-DOPA delivery is reflected in ongoing efforts to engineer core–shell and hybrid gold nanosystems with redox-protective and controlled-release properties for Parkinson's disease therapy,[11] underscoring the timeliness of establishing a robust *in vivo* safety baseline for such platforms. Using healthy male and female Wistar Han rats, we performed a comparative *in vivo* evaluation of free L-DOPA, adamantane- and PGM-AuNPs, and their corresponding formulations pre-incubated with L-DOPA following repeated oral administration. By integrating biodistribution, haematology, clinical biochemistry, and oxidative stress biomarkers, the study aimed to determine how AuNP surface chemistry and drug loading influence systemic biological responses and to establish the preclinial safety profile of these nanocarrier platforms before efficacy evaluation in disease models.

MATERIALS AND METHODS

AuNP Synthesis and Characterisation

AuNP formulations were synthesised by sodium borohydride reduction of hydrogen tetrachloroaurate ($HAuCl_4$) in the presence 1-adamantylamine (Ad-AuNPs) or peptidoglycan monomer (PGM-AuNPs), as previously described by Kalčec et al.[8] The abbreviations Ad-AuNPs and PGM-AuNPs are used throughout to distinguish the two formulations according to the ligand employed during synthesis; direct spectroscopic confirmation and quantitative determination of ligand coverage were not performed. Following synthesis, AuNPs were purified by centrifugation, resuspended in ultrapure water, and stored at 4 °C until use.

Comprehensive physicochemical characterisation of both AuNP formulations has also been reported previously.[8,9] Briefly, elemental gold concentration was determined by graphite furnace atomic absorption spectrometry (GFAAS), while hydrodynamic diameter, polydispersity index (PDI), and ζ-potential were measured using dynamic and electrophoretic light scattering (DLS/ELS). Nanoparticle morphology and primary particle size were evaluated by transmission electron microscopy (TEM), and colloidal stability was assessed in ultrapure water (UPW) and complete cell culture medium. Stock suspensions were diluted in UPW to the required concentrations immediately before administration.

AuNP formulations pre-incubated with L-DOPA were prepared according to the loading procedure established previously.[8] Briefly, PGM-AuNPs or Ad-AuNPs were incubated with L-DOPA for 30 min before administration. Following incubation, the nanoparticles were not separated from unbound L-DOPA, and the complete incubation mixture was used for oral administration. The formulations were adjusted to provide 0.4 mg Au kg^{-1} body weight and a total L-DOPA dose of 10 mg kg^{-1} body weight. Thus, 10 mg kg^{-1} refers to the total L-DOPA present in the administered formulation rather than to nanoparticle-associated L-DOPA. Based on the previously determined loading efficiencies,[8] only a fraction of the administered L-DOPA was associated with the AuNPs, with a higher associated fraction for PGM-AuNPs than for Ad-AuNPs.

Animal Experiments

All animal experiments were approved by the Ethical Committee of the Croatian Ministry of Agriculture, Directorate of Veterinary and Food Safety, Department of Animal Welfare (Ethical Committee review number EP 222/2019; Animal Welfare approval class UP/I-322-01/19-01/61, URBR: 525-10/0543-19-5). Animal care was carried out in accordance with the EU Directive 2010/63/EU for animal experiments, with the Animal Protection Act (OG 135/06, 37/13) and with the Ordinance on the protection of animals used for experimental and other scientific purposes (OG 55/13). According to the recommendations of the European Society of Gender Health and Medicine, both sexes were included in the study: gender-specific differences were expected.

Wistar rats of both sexes, aged 12 weeks and weighing 320–350 g body weight (b.w.) for males (M) and 190–220 g b.w. for females (F), were bred under specific pathogen-free (SPF) conditions at the Animal Breeding Unit, Institute for Medical Research and Occupational Health (IMROH), Zagreb, Croatia. Animals were acclimated in a controlled environment (temperature: 23 ± 2 °C; humidity: 55 ± 7 % and light: 12 h light / dark cycle) and fed with standard GLP-certified food (Mucedola, 4RF21, Italy) and water ad libitum.

In total, 70 (35 F and 35 M) Wistar HsdBrlHan rats were used. Animals were randomly assigned to experimental groups to avoid any bias and treated daily by gavage with test substances. Dose selection for PGM-AuNPs included a high-dose arm (0.8 mg Au kg^{-1}) to establish a safety margin for the lead formulation, whereas Ad-AuNPs were evaluated only at the low dose (0.4 mg Au kg^{-1}). This reflects the substantially lower L-DOPA drug loading efficiency of Ad-AuNPs relative to PGM-AuNPs at equivalent gold concentrations (Kalčec et al., 2022); consequently, a gold-dose-matched high-dose Ad-AuNP arm would not correspond to a proportionally higher L-DOPA payload, limiting its relevance to the therapeutic objective of this study. Animals were divided into 7 groups per sex ($n = 5$ per group): (1) control (Ctl) group treated with physiological solution; (2) group treated with L-DOPA dose of 10 mg kg^{-1} b.w.; (3) group treated with low dose (LD; 0.4 mg Au kg^{-1}) of PGM-coated AuNPs, (4) group treated with high dose (HD; 0.8 mg Au kg^{-1}) of PGM-coated AuNPs; (5) group treated with PGM-AuNPs doped with L-DOPA at daily dose of 0.4 mg Au kg^{-1} + 10 mg L-DOPA kg^{-1} b.w.; (6) group treated with low dose (LD; 0.4 mg Au kg^{-1}) of Ad-coated AuNPs; (7) group treated with Ad-AuNPs doped with L-DOPA at daily dose of 0.4 mg Au kg^{-1} + 10 mg L-DOPA kg^{-1} b.w. All formulations were diluted in saline. Following 28 days of daily oral treatment administration, rats were sacrificed under general anaesthesia using an anaesthetic cocktail (Narketan, Vetoquinol UK Ltd., 80 mg kg^{-1} b.w.; Xylapan, Vetoquinol UK Ltd., 12 mg kg^{-1} b.w., i.p.) in order to avert any pain caused by exsanguinations and tissue harvesting. All gross pathological changes of the internal organs were examined by a licensed veterinarian. The blood samples were collected in heparinised vacutainers (Becton, Dickinson and Co., Rutherford, New Jersey, USA) by jugular venipuncture under general anaesthesia. After washing in ice-cold physiological saline, organs (liver, kidneys, brain) were weighed and divided into small pieces

weighing roughly 300 mg. Tissue samples used for the measurement of accumulated AuNPs were immediately frozen at −20 °C. Fresh tissue homogenates were used to analyse the oxidative stress response. Tissue homogenates were prepared in 0.05 M phosphate buffer solution (PBS, pH 7.4) containing 0.1 mM ethylenediaminetetraacetic acid (EDTA) using a motor-driven homogeniser on an ice bath.

Blood Analysis

Blood samples were collected by jugular venipuncture, using the Vacutainer blood collection system (Becton, Dickinson and Co., Rutherford, NJ). Serum was separated by centrifugation at 1000 × *g* at 4 °C for 15 min, within 1 h of collection, and aliquots were stored at −80 °C until analysis. Serum levels of total proteins (TP), total bilirubin (Bil-T), albumin (ALB). triglycerides (TG), uric acid (UA), total cholesterol (TC), glucose (GLU) and creatinine (CREA), as well as the activities of AST, ALP, CK and LDH, were determined by standard commercial reagent packages (Beckman Coulter Biomedical Ltd., O'Callaghans Mills, Ireland) with the Beckman Coulter AU 680 biochemical analyser (Beckman Coulter Biomedical Ltd. München, Germany).

Determination of Accumulated Gold in Organs

The total Au content in different organs and tissues was measured by ICP-MS after microwave-assisted acid digestion. An Agilent Technologies 7500cx ICP-MS system (Agilent, Waldbronn, Germany) equipped with an integrated auto-sampler, a Scott Quartz spray chamber and a MicroMist nebuliser (Glass expansion, Australia) was used. According to Agilent Technologies' recommendations, operating conditions were normal for general and high matrix analysis. The tuning solution (Agilent Technologies, Japan) containing 10 µg L^{-1} of Li, Y, Ce, Tl and Co in 2 % (*w* / *v*) HNO_3 was used daily in order to achieve satisfying intensities for both oxide ions and doubly charged ones as well as to obtain lower yields. Calibration of the ICP-MS system was performed by the external standards method, using calibration standards prepared from stock elemental standard solutions of 1000 mg L^{-1} from Merck (Darmstadt, Germany) and internal standards of Rh and Lu. "Internal standard stock solution" was added to both samples and standards to achieve the final concentration of 10 µg L^{-1}. Before each series of samples, a reagent blank was measured to ensure contamination control. Calibration curves were created linearly after deduction of the reagent blank. Tissue samples were digested in the quartz digestion vessels with the microwave UltraCLAVE IV Milestone digestion device (MLS GmbH Mikrowellen-Laborsysteme, Leutkirch, Germany). Prior to irradiation at 800 W and 120 °C for 10 min, Suprapur 65 % HNO_3 (Merck, Darmstadt, Germany) was added to the precisely weighed tissue samples, followed by irradiation at 1600 W and 250 °C for 30 min.

This resulted in the absolute and almost concurrent dissolution of tissue samples to colourless solutions. The same microwave procedure was used to prepare a set of digestion blanks. Additionally, after cooling the vessels, ultrapure water was added to the final volume of 50 mL, which resulted in the overall dilution of 200 *v* / *m* and the final solution comprising 10 % *v* / *v* HNO_3. All data are expressed as total Au concentration, in mg Au per kg of wet tissue.

Evaluation of Oxidative Stress Response

Intracellular ROS in tissue homogenates were measured using 2',7'-dichlorofluorescin diacetate (DCFH-DA) and dihydroethidium (DHE) staining assays. In the presence of a superoxide radical, DHE is oxidised to a fluorescent 2-hydroethidium allowing the accurate measurement of fluorescence signals which correlate with the amount of superoxide radical. DCFH-DA is converted by cellular esterase into non-fluorescent 2'7'-dichlorofluorescin (DCFH), which is then oxidised to the fluorescent DCF product in the presence of hydroxyl radical. The procedures were performed as previously described.[12] An ice-cold 40 mM Tris–HCl buffer (pH 7.4) was used for diluting fresh 10 % (*w* / *v)* tissue homogenates to 0.25 % (*w* / *v*) homogenates, which were pipetted into wells of a 96-well plate following the addition of 20 µL 0.12 mM DCFH-DA or DHE. Autofluorescence was examined by preparing the tissue without the addition of a dye. After incubating the samples for 20 min at 37 °C fluorescence was determined at the 488 nm excitation and 525 nm emission wavelengths using a fluorescence plate reader Victor3™ (Perkin Elmer, Shelton, USA).

A monochlorobimane (MBCl) fluorescent probe, highly specific for glutathione (GSH) detection, was used for measuring the GSH level in tissue. Diluted 0.25 % (*w* / *v*) tissue homogenates were prepared in the 40 mM Tris–HCl buffer (pH 7.4) and placed on ice prior to analysis. Furthermore, 0.1 mL of 0.25 % homogenate portions was pipetted into wells of a 96-well plate following the addition of 20 µL of 0.24 mM MBCl. Autofluorescence was examined by preparing the tissue without the addition of a fluorescent probe. All samples were incubated for 30 min at 37 °C. Fluorescence was determined at the 355 nm excitation and 460 nm emission wavelengths using a Victor3™ plate reader. QuantiPro BCA assay kit (QPBCA, Merck KGaA, Darmstadt, Germany) was used for protein quantification according to the manufacturer's instructions. Results are expressed as relative fluorescence units normalized to total protein content (RFU / mg protein) and are presented as mean ± SD (n = 5 animals per sex and treatment group). Significant differences ($p < 0.05$) between controls and treated animals are indicated by the asterisks (*).

Table 1. Physicochemical characteristics relevant for the *in vivo* evaluation of gold nanoparticles coated with 1-adamantylamine (Ad-AuNPs) and peptidoglycan monomer (PGM-AuNPs) formulations. Primary size (d_{TEM}, n = 100) determined by transmission electron microscopy (TEM), zeta potential (ζ) measured by electrophoretic light scattering (ELS), hydrodynamic diameter (d_H) and polydispersity index (PDI) by dynamic light scattering (DLS).

Property	Ad–AuNPs	PGM–AuNPs	Method
*d*TEM / nm	25.1 ± 3.2	25.6 ± 2.7	TEM
d_H / nm	74.8 ± 6.5	68.4 ± 8.3	DLS
PDI	0.18	0.21	DLS
ζ potential / mV	–28.8 ± 4.3	–31.4 ± 6.7	ELS

Statistical Analysis

GraphPad Prism (version 9.0.0, GraphPad Software, San Diego, CA, USA) was used for all statistical analyses and the graphical representation of the results. Data were screened for potential outliers using the robust regression and outlier removal (ROUT) test (Q = 1 %). No data points were identified as outliers and excluded from the final analyses. Differences between experimental groups were evaluated using two-way analysis of variance (two-way ANOVA) to assess the main effects of treatment and sex, as well as their interaction (treatment × sex). When significant main effects were detected, post hoc multiple comparison tests were applied. Tukey's multiple comparisons test was used to compare differences between treatment groups, while Šidák's test for multiple comparisons was used to evaluate differences between sexes. A significant treatment × sex interaction was interpreted as evidence that the treatment response differed between sexes, whereas a significant main effect of sex in the absence of a significant interaction was interpreted as an overall difference between males and females irrespective of treatment. Results are presented as mean ± standard deviation (SD). The sample size for each group is indicated in the corresponding figure legends. Statistical significance was set at $p < 0.05$.

RESULTS AND DISCUSSION

Characteristics of AuNPs

The physicochemical properties of Ad-AuNPs and PGM-AuNPs have been comprehensively described in our previous study[8] and are summarised in Table 1 for completeness. Both AuNPs formulations exhibited comparable spherical morphology, primary particle size (~24 nm), hydrodynamic diameter and ζ-potential.

Although Ad-AuNPs and PGM-AuNPs exhibited similar size, morphology, and surface charge, their surface chemistry resulted in markedly different interactions with L-DOPA. Drug loading efficiency (DLE) experiments demonstrated that PGM-AuNPs consistently achieved approximately two-fold higher L-DOPA loading than Ad-AuNPs at both tested nanoparticle concentrations,[8] indicating that the PGM coating provides a more favourable interface for drug adsorption. The maximum DLE was obtained after 30 min of incubation, and this protocol was therefore used for the preparation of L-DOPA-pre-incubated AuNPs employed in the present *in vivo* study.

Serum Biochemistry

Serum biochemical parameters were analysed to evaluate potential systemic effects of repeated oral administration of free L-DOPA, Ad-AuNPs and PGM-AuNPs alone, and their formulations with L-DOPA (Fig. 1).

Among the tested nanocarrier formulations, biochemical alterations were most evident following administration of Ad-AuNPs, whereas PGM-AuNPs exhibited a largely unaltered biochemical profile.

Two-way ANOVA revealed significant treatment effects for serum AST ($p < 0.001$), ALP ($p < 0.001$), TP ($p < 0.05$), Bil-T ($p < 0.01$), LDH ($p < 0.0001$), and creatinine (CREA; $p < 0.0001$). Significant effects of sex were observed for ALP ($p < 0.0001$) and Bil-T ($p < 0.05$), while a significant treatment × sex interaction was detected only for CREA ($p < 0.0001$), indicating that the treatment-related response for this parameter differed between males and females. Serum TG and UA were influenced by sex but not by treatment, whereas ALB, CK, TC, and GLU remained unaffected (Supplementary Figure S1).

Post hoc analyses demonstrated that treatment-related biochemical alterations were generally mild and were predominantly associated with the Ad-AuNPs formulation. Administration of free L-DOPA resulted in a modest increase in Bil-T compared with controls. In contrast, neither the low nor the high dose of PGM-AuNPs alone produced significant changes in any of the analysed biochemical parameters. The combination of PGM-AuNPs with L-DOPA induced a significant increase in ALP, which was restricted to male animals.

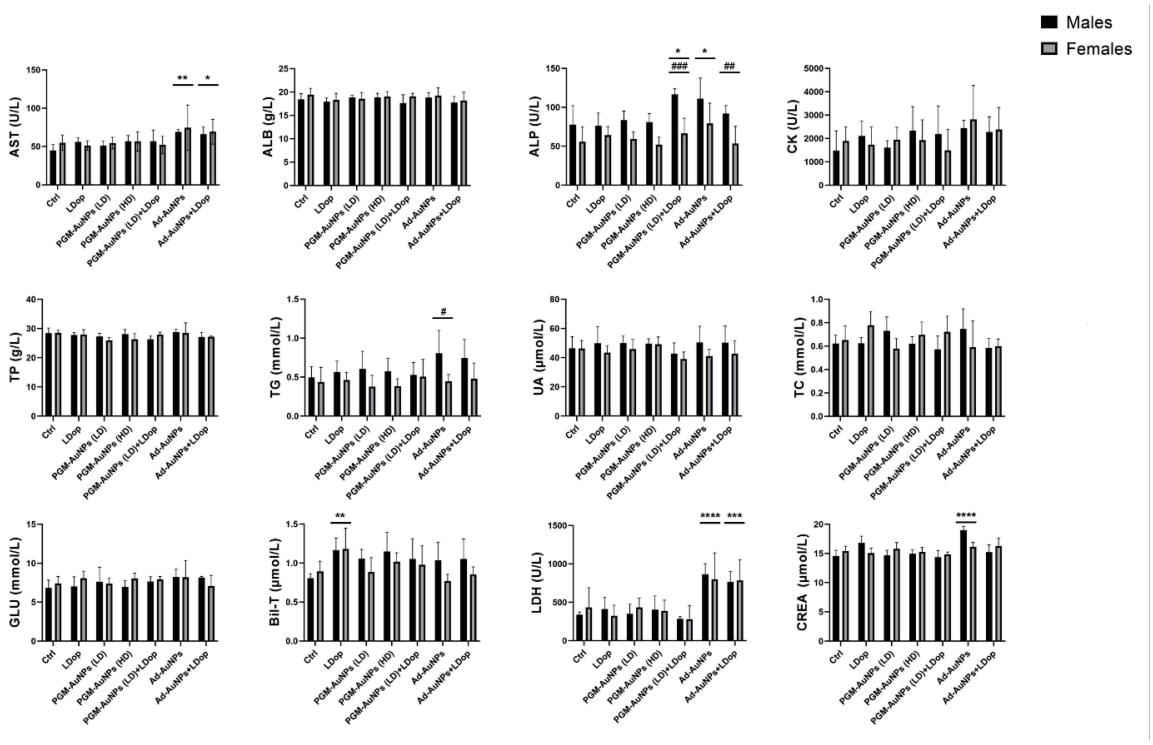


Figure 1. Biochemical parameters in the serum of the control rats (Ctrl) and rats treated with L-DOPA (LDop), low dose (LD) of peptidoglycan monomer-coated gold nanoparticles (PGM-AuNPs, high dose (HD) of PGM-AuNPs, combination of LD PGM-AuNPs and LDop, adamantane-coated AuNPs (Ad-AuNPs), and combination of Ad-AuNPs + LDop. The following parameters were measured: AST – aspartate aminotransferase; ALB – albumin; ALP – alkaline phosphatase; CK – creatine kinase; TP – total protein; TG – triglycerides; UA – uric acid; TC – total cholesterol; GLU – glucose; Bil-T – total bilirubin; LDH – lactate dehydrogenase; CREA – creatinine. Data are presented as mean ± SD (n = 5 rats per group). Statistical analysis was performed using two-way ANOVA followed by appropriate post hoc tests. * $p < 0.05$, ** $p < 0.01$, *** $p < 0.001$, **** $p < 0.0001$, indicate significant differences between the treatment and the Ctrl group; # $p < 0.05$, ## $p < 0.01$, ### $p < 0.001$, indicate significant sex differences in the same treatment group.

The most pronounced biochemical changes were observed following administration of Ad-AuNPs. Both Ad-AuNPs and- Ad-AuNPs with L-DOPA significantly increased serum AST and LDH activities compared with controls, suggesting a mild treatment-related effect on tissue integrity. In addition, Ad-AuNPs alone increased ALP and creatinine concentrations, with these effects being more evident in males. The most pronounced biochemical changes were observed following administration of Ad-AuNPs. Both Ad-AuNPs and L-DOPA + Ad-AuNPs significantly increased serum AST and LDH activities compared with controls. In addition, Ad-AuNPs alone increased ALP and creatinine concentrations, with these effects being more evident in males. Although statistically significant, these changes should be interpreted in the context of their magnitude and the overall biochemical response rather than as isolated indicators of organ toxicity. The alterations were generally modest and were not accompanied by coordinated changes across functionally related biochemical parameters. In particular, the increases in AST and LDH observed following Ad-AuNP and Ad-AuNP + L-DOPA administration were not accompanied by significant changes in albumin or total bilirubin within these treatment groups, arguing against a coordinated pattern of impaired hepatic function, while the increase in creatinine was treatment- and sex-dependent rather than part of a broader pattern of renal dysfunction. Moreover, these biochemical changes were not associated with a consistent increase in ROS, depletion of GSH, or other evidence of sustained oxidative injury in the corresponding tissues. Considering the known dependence of clinical chemistry values on rat strain, sex, age, and analytical methodology, individual values were therefore interpreted relative to concurrent sex-matched controls rather than against a single universal reference interval. Taken together, the magnitude and isolated nature of the observed changes support their interpretation as mild biological responses rather than evidence of overt organ toxicity.

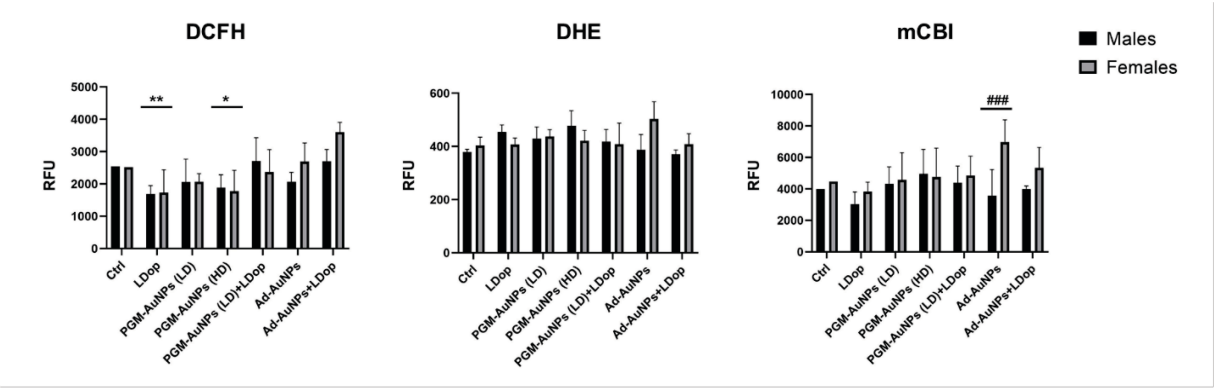


Figure 2. Evaluation of oxidative stress in the brain of the control rats (Ctrl) and rats treated with L-DOPA (LDop), low dose of peptidoglycan monomer (PGM)-coated gold nanoparticles (PGM-AuNPs (LD)), high dose of PGM-coated AuNPs (PGM-AuNPs (HD)), combination of PGM-AuNPs (LD) with L-DOPA (PGM-AuNPs (LD)+LDop), adamantane-coated AuNPs (Ad- AuNPs), and combination of Ad- AuNPs with L-DOPA (Ad-AuNPs+LDop). DCFH - 2',7'-dichlorofluorescein diacetate; DHE – dihydroethidium; mCBI – monochlorobimane; RFU – relative fluorescence units. Data are presented as mean ± SD (n = 5 rats per group). Statistical analysis was performed using two-way ANOVA followed by appropriate post hoc tests. * $p < 0.05$, ** $p < 0.01$ indicate significant differences between the treatment and the Ctrl group; ### $p < 0.001$ indicates significant sex differences in the same treatment group.

Oxidative Stress Response

Oxidative stress responses were evaluated in the brain, kidneys, liver, and serum by measuring overall reactive oxygen species (ROS; DCFDA), superoxide production (DHE), and reduced glutathione (GSH; mCBI) (Figures 2–5). Overall, repeated oral administration of AuNP formulations induced only modest, tissue-specific alterations in redox homeostasis, with no consistent pattern indicative of sustained oxidative stress.

In the brain (Fig. 2), two-way ANOVA revealed significant treatment effects for ROS ($p < 0.0001$), superoxide production ($p < 0.05$), and GSH levels ($p < 0.05$). Significant treatment × sex interactions were observed for superoxide and GSH, indicating that treatment-related responses for these endpoints differed between males and females. Post hoc analysis showed significantly reduced ROS levels in animals treated with free L-DOPA and the high dose of PGM-AuNPs compared with controls. Ad-AuNP treatment produced opposite effects on GSH levels in males and females, resulting in the observed interaction, whereas no evidence of increased oxidative burden was detected.

In the kidneys (Fig 3), treatment significantly affected ROS levels ($p < 0.0001$), with additional main effects of sex ($p < 0.0001$) and treatment × sex interaction ($p < 0.0001$). Animals treated with free L-DOPA as well as low- and high-dose PGM-AuNPs exhibited significantly lower ROS levels than controls. In contrast, no significant treatment-related changes were observed for superoxide production or GSH levels, indicating preservation of renal antioxidant capacity despite measurable nanoparticle accumulation.

In the liver (Figure 4), treatment significantly influenced ROS ($p < 0.0001$) and GSH levels ($p < 0.05$), while significant effects of sex were observed for both parameters. Treatment × sex interactions were detected for ROS, superoxide, and GSH, demonstrating that treatment-related responses for these redox endpoints differed between males and females. Post hoc analysis revealed significantly reduced ROS levels following treatment with free L-DOPA, both doses of PGM-AuNPs, L-DOPA -loaded PGM-AuNPs, and Ad-AuNPs. Increased GSH levels were observed only in the free L-DOPA and Ad-AuNP groups. Males generally exhibited higher hepatic GSH levels than females, and treatment-related effects were more pronounced in males.

In serum (Figure 5), treatment significantly affected ROS levels ($p < 0.01$), whereas sex influenced both ROS ($p < 0.05$) and superoxide production ($p < 0.01$). No treatment × sex interactions were detected. ROS levels were significantly reduced in animals treated with free L-DOPA the high dose of PGM-AuNPs, and Ad-AuNPs compared with controls. Although females exhibited higher overall superoxide levels than males, particularly in the Ad-AuNP-treated groups, treatment itself did not significantly affect this parameter. Serum GSH levels remained unchanged across all experimental groups.

Overall, the redox responses were tissue- and endpoint-specific. Significant treatment × sex interactions for selected endpoints in the brain, kidneys, and liver indicate that some treatment-related redox responses differed between males and females. However, these effects did not constitute a consistent pattern of increased ROS

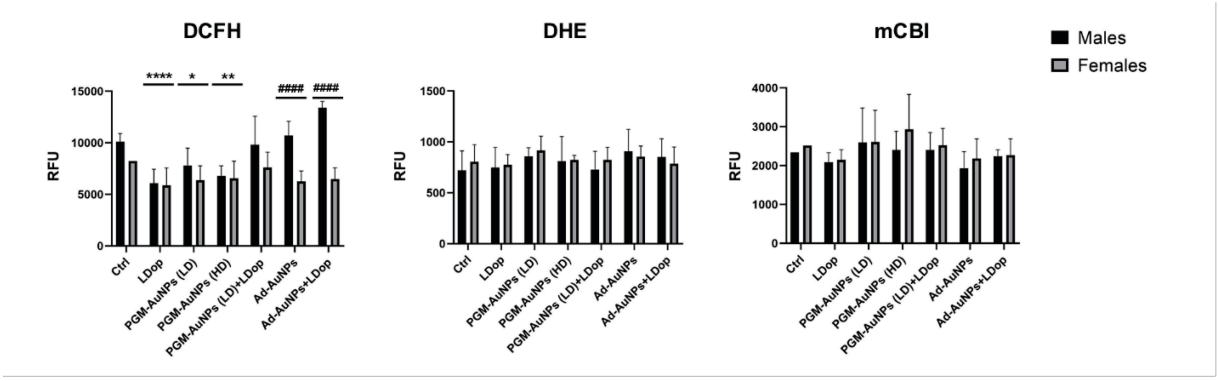


Figure 3. Evaluation of oxidative stress in kidneys of the control rats (Ctrl) and rats treated with L-DOPA (LDop), low dose of peptidoglycan monomer (PGM)-coated gold nanoparticles (PGM-AuNPs (LD)), high dose of PGM-coated AuNPs (PGM-AuNPs (HD)), combination of PGM-AuNPs (LD) with L-DOPA (PGM-AuNPs (LD)+LDop), adamantane-coated AuNPs (Ad- AuNPs), and combination of Ad- AuNPs with L-DOPA (Ad-AuNPs+LDop). DCFH - 2',7'-dichlorofluorescein diacetate; DHE – dihydroethidium; mCBI – monochlorobimane; RFU – relative fluorescence units. Data are presented as mean ± SD (n = 5 rats per group). Statistical analysis was performed using two-way ANOVA followed by appropriate post hoc tests. * $p < 0.05$, ** $p < 0.01$, **** $p < 0.0001$, indicate significant differences between the treatment and the Ctrl group; #### p < 0.0001 indicates significant sex differences in the same treatment group.

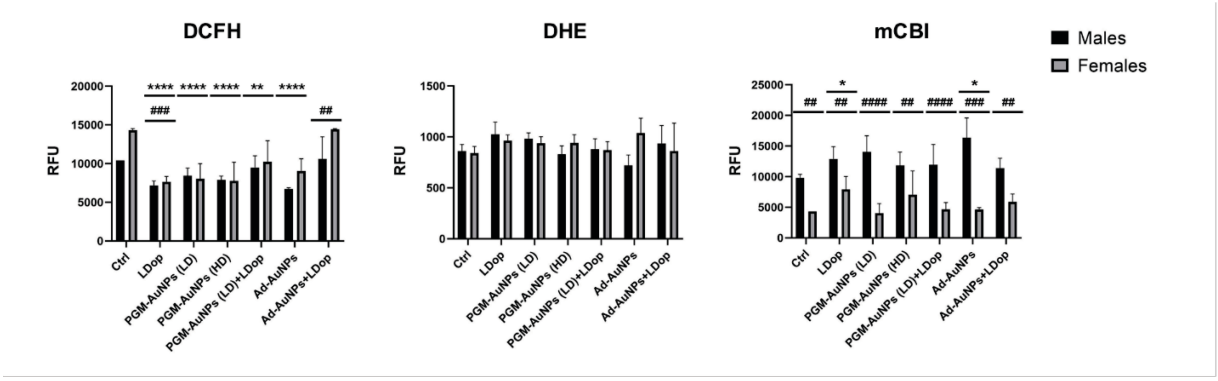


Figure 4. Evaluation of oxidative stress in the liver of the control rats (Ctrl) and rats treated with L-DOPA (LDop), low dose of peptidoglycan monomer (PGM)-coated gold nanoparticles (PGM-AuNPs (LD)), high dose of PGM-coated AuNPs (PGM-AuNPs (HD)), combination of PGM-AuNPs (LD) with L-DOPA (PGM-AuNPs (LD)+LDop), adamantane-coated AuNPs (Ad- AuNPs), and combination of Ad- AuNPs with L-DOPA (Ad-AuNPs+LDop). DCFH - 2',7'-dichlorofluorescein diacetate; DHE – dihydroethidium; mCBI – monochlorobimane; RFU – relative fluorescence units. Data are presented as mean ± SD (n = 5 rats per group). Statistical analysis was performed using two-way ANOVA followed by appropriate post hoc tests. * $p < 0.05$, ** $p < 0.01$, **** $p < 0.0001$, indicate significant difference between the treatment and the Ctrl group; ## $p < 0.01$, ### $p < 0.001$, #### $p < 0.0001$, indicate significant sex differences in the same treatment group.

accompanied by GSH depletion across tissues and treatments, arguing against sustained systemic oxidative stress. Contrary to the widely accepted paradigm that engineered nanoparticles induce oxidative stress through excessive ROS generation, repeated oral exposure to PGM-AuNPs did not produce a coordinated pro-oxidant response. Instead, ROS levels were frequently reduced, while GSH concentrations remained stable or increased in selected tissues. A comparable adaptive response has recently been described for orally administered gold and other inorganic nanoparticles, where low-dose, sub-cytotoxic exposure was shown to trigger a protective antioxidant transcriptional response in hepatocytes rather than sustained oxidative damage.[13] This is consistent with the broader concept of nanoparticle-induced hormesis, in which low, non-cytotoxic doses elicit biphasic, adaptive redox responses rather than the monotonic pro-oxidant effects assumed at higher exposure levels.[14] These findings suggest that the administered doses did not overwhelm endogenous antioxidant defence systems and may instead reflect such an adaptive redox response rather than oxidative damage.

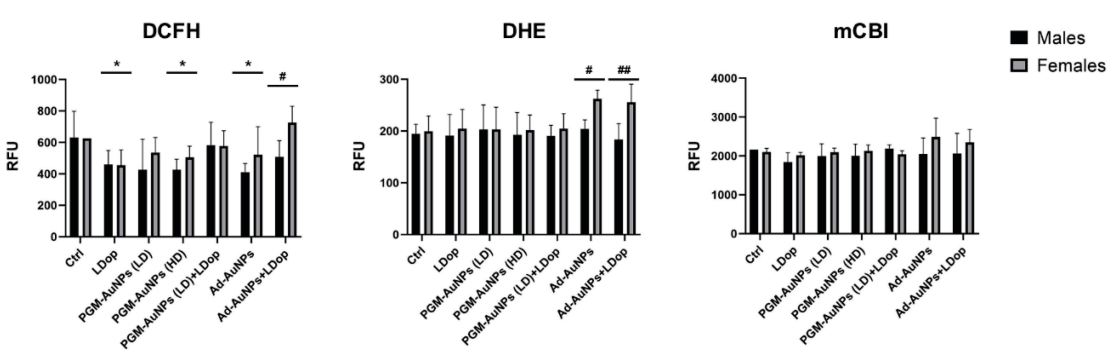


Figure 5. Evaluation of oxidative stress in the serum of the control rats (Ctrl) and rats treated with L-DOPA (LDop), low dose of peptidoglycan monomer (PGM)-coated gold nanoparticles (PGM-AuNPs (LD)), high dose of PGM-coated AuNPs (PGM-AuNPs (HD)), combination of PGM-AuNPs (LD) with L-DOPA (PGM-AuNPs (LD)+LDop), adamantane-coated AuNPs (Ad- AuNPs), and combination of Ad- AuNPs with L-DOPA (Ad-AuNPs+LDop). DCFH - 2',7'-dichlorofluorescein diacetate; DHE – dihydroethidium; mCBI – monochlorobimane; RFU – relative fluorescence units. Data are presented as mean ± SD (n = 5 rats per group). Statistical analysis was performed using two-way ANOVA followed by appropriate post hoc tests. * $p < 0.05$ indicates significant difference between the treatment and the Ctrl group; # $p < 0.05$, ## $p < 0.01$, indicate significant sex differences in the same treatment group.

Tissue Accumulation

Inductively coupled plasma mass spectrometry (ICP-MS) was used to quantify gold concentrations in the brain, kidneys, liver, and lungs following repeated oral administration of AuNP formulations (Fig. 6). Gold accumulation was strongly dependent on treatment and was detected predominantly in the kidneys, followed by the liver and lungs. Two-way ANOVA revealed significant treatment effects for gold concentrations in the kidneys ($p < 0.0001$), liver ($p < 0.0001$), and lungs ($p < 0.0001$), whereas no significant effects of sex or treatment × sex interactions were observed.

Post hoc analysis demonstrated that animals receiving the high dose of PGM-AuNPs exhibited significantly higher gold concentrations in the kidneys, liver, and lungs than all other experimental groups (Fig. 6), indicating dose-dependent tissue accumulation following repeated oral exposure. In contrast, gold concentrations in animals treated with the low dose of PGM-AuNPs and Ad-AuNPs or the corresponding L-DOPA -containing formulations were below the analytical limit of detection or remained at background levels and did not differ significantly from controls. Figure 6 therefore focuses on the PGM-AuNP dose-response, for which measurable accumulation was observed at the high dose. Gold concentrations in the Ad-AuNP and Ad-AuNP + L-DOPA groups were below the analytical limit of detection in the analysed tissues and were therefore not plotted in Figure 6. No significant main effect of sex or treatment × sex interaction was observed for tissue gold concentrations, indicating no statistical evidence of sex-dependent differences in gold biodistribution under the conditions of this study.

ICP-MS analysis demonstrated a clear organ-specific biodistribution pattern following repeated oral administration of PGM-AuNPs. The highest gold concentrations were detected in the kidneys, followed by the liver and lungs, whereas no measurable gold was detected in the brain. The predominance of renal accumulation suggests that the absorbed fraction of the AuNP, or their degradation products, is efficiently processed through the renal excretory pathway. This is consistent with prior biokinetic work showing that, unlike intravenously administered AuNPs, which distribute broadly to liver, spleen, and lung, orally administered AuNPs accumulate predominantly in the kidney, implicating the renal route as the principal clearance pathway following gastrointestinal absorption.[15] At the same time, accumulation in the liver is consistent with the well-established role of the mononuclear phagocyte (reticuloendothelial) system in the sequestration and clearance of circulating nanoparticles.

Despite the intended application of these formulations as brain-targeted nanocarriers, gold concentrations in brain tissue remained below the detection limit after 28 days of repeated oral administration. This finding suggests that, under physiological conditions in healthy animals, oral exposure alone does not result in measurable nanoparticle accumulation within the central nervous system. This observation is not unexpected, considering the highly restrictive nature of the blood-brain barrier and the absence of pathological conditions that could facilitate nanoparticle transport into the brain. Importantly, the present study was designed to establish the systemic safety profile of the nanocarrier platform rather than to evaluate delivery efficiency under disease conditions, where blood-brain barrier permeability and nanoparticle uptake may differ substantially.

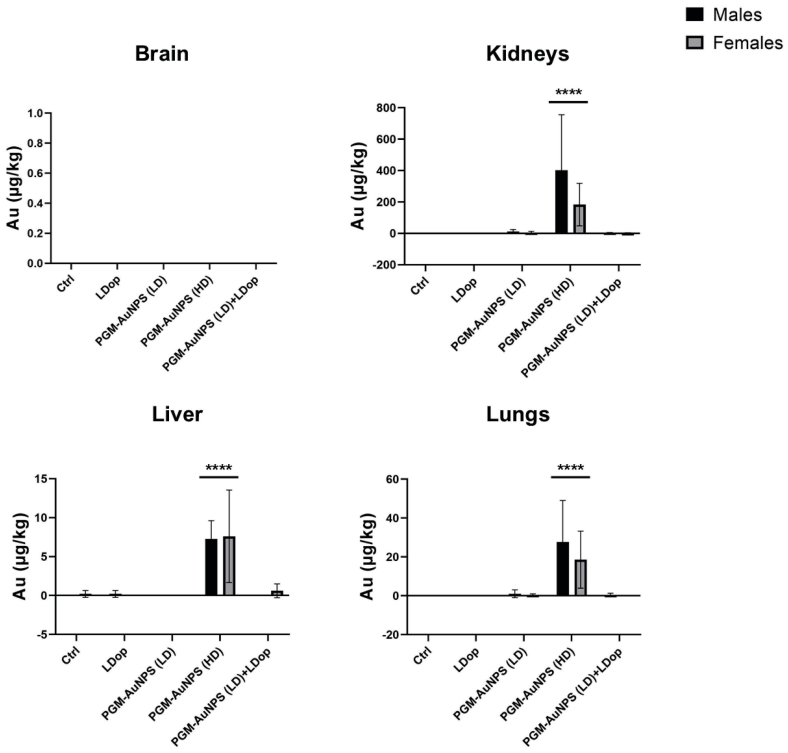


Figure 6. Gold concentrations measured using inductively coupled plasma mass spectrometry (ICP–MS) in the brain, kidneys, liver, and lungs of the control rats (Ctrl) and rats treated with L-DOPA (LDop), low dose (LD) and high dose (HD) of peptidoglycan monomer (PGM)-stabilised gold nanoparticles (PGM-AuNPs), and combination of PGM-AuNPs with L-DOPA (PGM-AuNPs (LD)+LDop). Data are presented as mean ± SD (n = 5 rats per group). Statistical analysis was performed using two-way ANOVA followed by appropriate post hoc tests. **** $p < 0.0001$ indicates significant difference between the treatment and the Ctrl group.

Interestingly, loading PGM-AuNPs or Ad-AuNPs with L-DOPA did not result in increased gold accumulation in any of the analysed organs, indicating that drug conjugation did not substantially alter nanoparticle biodistribution following oral administration. This suggests that the observed tissue distribution was governed primarily by the physicochemical characteristics of the nanoparticle carrier rather than by the presence of the therapeutic cargo.

The absence of significant treatment × sex interactions in gold biodistribution contrasts with the pronounced sex-dependent effects observed for serum biochemistry and oxidative stress parameters in this study, and with reports of marked sex differences in the tissue handling of other metal-based nanoparticles, including orally administered silver nanoparticles in Wistar rats.[12] Sex-related differences in xenobiotic absorption, plasma protein binding, and renal and hepatic clearance are well documented across toxicological contexts generally [16] and have been specifically linked to sex-specific protein corona formation and immune handling in nanomedicine,[17] which may account for the sex-dependent biochemical and redox responses reported here despite comparable gold body burden between males and females.

Although animals receiving the high dose of PGM-AuNPs accumulated significantly greater amounts of gold than the other treatment groups, this increased tissue burden was not accompanied by corresponding alterations in serum biochemistry, oxidative stress biomarkers, or overt systemic toxicity. The decision to restrict Ad-AuNP testing to a single dose was based on its markedly lower L-DOPA loading efficiency relative to PGM-AuNPs at equivalent gold concentrations,[8] meaning that a gold-dose-matched escalation would not deliver a proportionally greater L-DOPA payload. This choice is further supported by the present findings, in which even the tested dose of Ad-AuNPs produced more pronounced biochemical alterations than either PGM-AuNP dose, suggesting limited additional translational benefit from dose escalation of the Ad-AUNPs formulation. These findings indicate that tissue accumulation alone is not necessarily predictive of adverse biological

effects. Instead, they support the concept that the biological response to engineered nanoparticles is determined by a complex interplay of factors, including dose, surface stabilisation, physicochemical properties, and interactions with biological systems, rather than by tissue concentration alone. The favourable safety profile observed despite measurable organ accumulation therefore supports the continued preclinical development of PGM-AuNPs as oral drug delivery vehicles.

Integrated Toxicological Profile of Surface–Engineered AuNPs

To facilitate comparison between nanoparticle formulations, the principal treatment-related changes observed across biodistribution, serum biochemistry, and oxidative stress endpoints are summarized in Figure 7.

Overall, repeated oral administration of PGM-AuNPs produced a favourable toxicological profile. Although the high-dose PGM-AuNP formulation resulted in the greatest tissue accumulation, particularly in the kidneys and liver, this was not associated with corresponding disturbances in serum biochemical markers or oxidative stress parameters. In contrast, Ad-AuNPs elicited more consistent alterations in liver- and kidney-related biochemical markers, together with tissue-specific changes in redox homeostasis. Thus, the biological response was not predicted by tissue gold burden alone and differed between the two AuNP formulations. As these formulations were synthesised using different surface ligands, the observed differences are consistent with an important contribution of surface chemistry to their biological behaviour; however, direct attribution to ligand identity or surface coverage would require surface-sensitive characterization. Pre-incubation with L-DOPA did not substantially alter gold biodistribution or the overall systemic safety profile of either AuNP formulation.

CONCLUSION

This study provides the first comparative *in vivo* safety evaluation of two rationally designed, surface-engineered gold nanoparticle (AuNP) platforms developed for oral L-DOPA delivery. Repeated oral administration of PGM-AuNPs and Ad-AuNPs, either alone or in formulations pre-incubated with L-DOPA, resulted in measurable, organ-specific gold accumulation, predominantly in the kidneys and liver, without detectable accumulation in the brain. Importantly, despite dose-dependent accumulation of PGM-AuNPs, particularly in clearance organs, tissue burden was not accompanied by widespread biochemical disturbances, oxidative stress, or overt systemic toxicity.

The comparative design demonstrated that tissue gold burden alone did not predict the biological response.

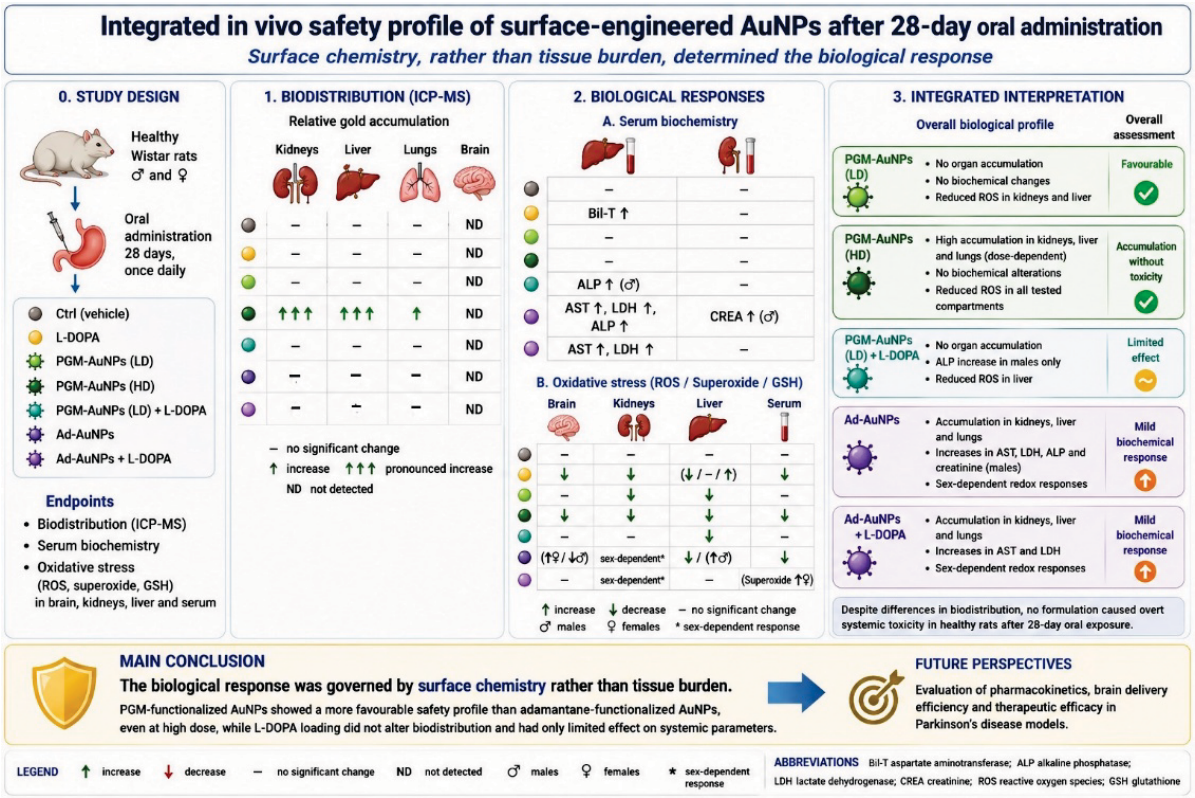


Figure 7. Integrated *in vivo* safety profile of surface-engineered AuNPs after 28-day oral administration.

Despite their comparable primary size, morphology, hydrodynamic diameter, and ζ-potential, the two AuNP formulations elicited distinct *in vivo* responses, with PGM-AuNPs displaying a more favourable safety profile than Ad-AuNPs. As the formulations were synthesised using chemically distinct ligands, these findings are consistent with an important contribution of surface chemistry to their biological behaviour; however, direct attribution of the observed differences to ligand identity or surface coverage requires further surface-sensitive characterization. Pre-incubation of the AuNP formulations with L-DOPA did not substantially alter gold biodistribution or their overall systemic safety profile. However, because unbound L-DOPA was not removed before administration, the present study does not distinguish biological effects attributable to nanoparticle-associated L-DOPA from those of the unbound drug fraction.

Collectively, these findings demonstrate that conventional physicochemical descriptors and tissue gold burden alone are insufficient to predict the *in vivo* biological performance of AuNP-based nanocarriers. By extending our previous physicochemical and drug-loading studies to repeated-dose *in vivo* evaluation, the present work provides an important preclinical safety foundation for further development of PGM-AuNPs as L-DOPA nanocarriers. Future studies should determine their pharmacokinetic behaviour, L-DOPA delivery efficiency, including delivery to the brain, and therapeutic efficacy in relevant disease models.

Acknowledgment. This study was financially supported by the "Research Cooperability" Program of the Croatian Science Foundation funded by the European Union from the European Social Fund under the Operational Programme Efficient Human Resources 2014–2020 (grant HRZZ-PZS-2019-02-4323), by the European Regional Development Fund project KK.01.1.1.02.0007 "Research and Education Centre of Environmental Health and Radiation Protection – Reconstruction and Expansion of the Institute for Medical Research and Occupational Health" and the European Union – Next Generation EU programme (contract document designation 643-02/23-01/00016). We are grateful to Krunoslav Ilić and Barbara Pem for their technical help and assistance during experiments.

REFERENCES

[1] GBD 2021 Stroke Risk Factor Collaborators, *Lancet Neurol.* **2024**, *23*, 973–1003.

[2] W. M. Pardridge, *NeuroRx* **2005**, *2*, 3–14. https://doi.org/10.1602/neurorx.2.1.3

[3] D. Aarsland, L. Batzu, G. M. Halliday, G. J. Geurtsen, C. Ballard, K. R. Chaudhuri, D. Weintraub, *Nat. Rev. Dis. Primers* ***2021***, *7*, 47. https://doi.org/10.1038/s41572-021-00280-3

[4] J. Xie, Z. Shen, Y. Anraku, K. Kataoka, X. Chen, *Biomaterials* **2019**, *224*, 119491. https://doi.org/10.1016/j.biomaterials.2019.119491

[5] C. Saraiva, C. Praça, R. Ferreira, T. Santos, L. Ferreira, L. Bernardino, *J. Control. Release* **2016** *235*, 34–47. https://doi.org/10.1016/j.jconrel.2016.05.044

[6] S. Mitragotri, T. Lammers, Y. H. Bae, S. Schwendeman, S. De Smedt, J. Leroux, D. Peer, I. C. Kwon, H. Harashima, A. Kikuchi, Y. Oh, V. Torchilin, W. Hennink, J. Hanes, K. Park, *J. Control. Release* **2017**, *246,* 183–184. https://doi.org/10.1016/j.jconrel.2017.01.011

[7] D. M. Teleanu, I. Negut, V. Grumezescu, A. M. Grumezescu, R. I. Teleanu, *Nanomaterials* **2019**, *9*, 371. https://doi.org/10.3390/nano9030371

[8] N. Kalčec, N. Peranić, R. Barbir, C. R. Hall, T. A. Smith, M. A. Sani, R. Frkanec, F. Separovic, I. Vinković Vrček, *Spectrochim. Acta A Mol. Biomol. Spectrosc*. **2022**, *268*, 120707. https://doi.org/10.1016/j.saa.2021.120707

[9] I. Mamić, M. Beus, N. Kalčec, N. Peranić, R. Frkanec, P. Turčić, I. V. Vrček. *Croat. Chem. Acta* **2025**, *98*, 145–156. https://doi.org/10.5562/cca4172

[10] R. Barbir, R. R. Jiménez, R. Martín-Rapún, V. Strasser, D. Domazet Jurašin, S. Dabelić, J. M. De La Fuente, I. Vinković Vrček, *ACS Appl. Mater. Interfaces* **2021**, *13*, 27533–27547. https://doi.org/10.1021/acsami.1c04063

[11] A. Kowalska, K. Zima, P. Nowicka, *Dalton Trans*. **2025**, *54*, 17597–17610. https://doi.org/10.1039/D5DT02168E

[12] M. Ćurlin, R. Barbir, S. Dabelić, M. Ljubojević, W. Goessler, V. Micek, I. Žuntar, M. Pavić, L. Božičević, I. Pavičić, I. Vinković Vrček, *Part Fibre Toxicol* **2021**, *18*, 38. https://doi.org/10.1186/s12989-021-00425-y

[13] J. Cai, J. Peng, J. Feng, R. Li, P. Ren, X. Zang, Z. Wu, Y. Lu, L. Luo, Z. Hu, J. Wang, X. Dai, P. Zhao, J. Wang, M. Yan, J. Liu, R. Deng, D. Wang, *Nat. Commun*. **2023**, *14*, 3643. https://doi.org/10.1038/s41467-023-39423-3

[14] I. Iavicoli, V. Leso, L. Fontana, E. J. Calabrese, *Int. J. Mol. Sci.* **2018**, *19*, 805. https://doi.org/10.3390/ijms19030805

[15] M. Jo, S. Bae, M. Go, H. Kim, Y. Hwang, S. Choi, *Nanomaterials* **2015**, *5*, 835–850. https://doi.org/10.3390/nano5020835

[16] M. Gochfeld, *Toxicol Pathol.* **2017**, *45*, 172–189. https://doi.org/10.1177/0192623316677327

[17] M. Poley, G. Chen, N. Sharf-Pauker, A. Avital, M. Kaduri, M. Sela, P. M. Raimundo, L. Koren, S. Arber, E. Egorov, J. Shainsky, J. Shklover, A. Schroeder, *Adv. NanoBiomed Res.* **2022**, *2*, 2200089. https://doi.org/10.1002/anbr.202200089.